Research Article **AJSRE (2020), 5:25**

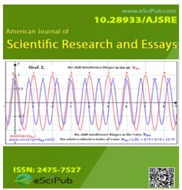

American Journal of Scientific Research and Essays
(ISSN:2475-7527)

Numerical simulation of propeller jet field based on Star-ccm+

Peng-rong Li

College of Ocean Science and Engineering, Shanghai Maritime University, Shanghai 201306, China.

ABSTRACT

During the ship's voyage, the propeller jet affects the movement of silt at the bottom of the bed. To research the influence of the bottom boundary on the propeller jet field, this paper takes the standard propeller DTRC4119 propeller as the research object and uses the CFD software Star-ccm+ to carry out a numerical simulation of the propeller jet under uniform flow. The flow velocity distribution of the jet under four operating conditions is mainly analyzed, including the axial velocity, tangential velocity and radial velocity of the jet. The results show that the distance between the propeller and the boundary does not affect the magnitude and distribution of the velocity on the initial plane but affects the shape of the axial velocity and the velocity on the central axis in the development zone; The closer to the bottom boundary, the greater the disturbance of tangential velocity and radial velocity, the peak value of tangential velocity will be affected and changed from central symmetry of velocity to unanimous trend earlier. The radial velocity contributes less to the overall velocity and can be ignored.

Keywords: Propeller; Jet field; CFD

***Correspondence to Author:**
Peng-rong Li
College of Ocean Science and Engineering, Shanghai Maritime University, Shanghai 201306, China.

How to cite this article:
Peng-rong Li. Numerical simulation of propeller jet field based on Star-ccm+. American Journal of Scientific Research and Essays, 2020, 5:25

eSciPub LLC, Houston, TX USA.
Website: http://escipub.com/

Introduction

Under water, the high-speed ship propellers will continuously push the water backward through the blades, so that the water generates forward thrust and pushes the ship forward. In this process may lead to the propeller scour river bed phenomenon aggravated, changing the distance between the seabed and the ship [1].

As early as 1950, Albertson et al [2] obtained an empirical formula for jet velocity by observing ordinary water jets and provided a theoretical basis for the subsequent research on ship propeller jets. In 1988, Whitehouse [3] predicts propeller jet caused seabed scour through investigation. Sumer et al. (2002) [4] found the relationship between propeller jet and seabed scour. Later, Stewart (1992) [5], Hamill and Johnston (1993) [6], Hashmi (1993) [7], Lam et al. (2011) [8] have made further research on the outflow velocity and velocity attenuation of the propeller jet flow field, and modified the Albertson empirical formula through physical model tests and numerical simulations, and obtained the propeller jet flow velocity formula and distribution law closer to the real situation.

The efflux velocity refers to the maximum axial speed on the initial plane and is expressed by Vo. The axial velocity distribution of the propeller jet has been summarized by researchers, as shown in Figure 1. It can be seen from the figure that the speed of the water body due to rotation on the propeller surface is the highest on the outflow plane, and then it begins to decay.

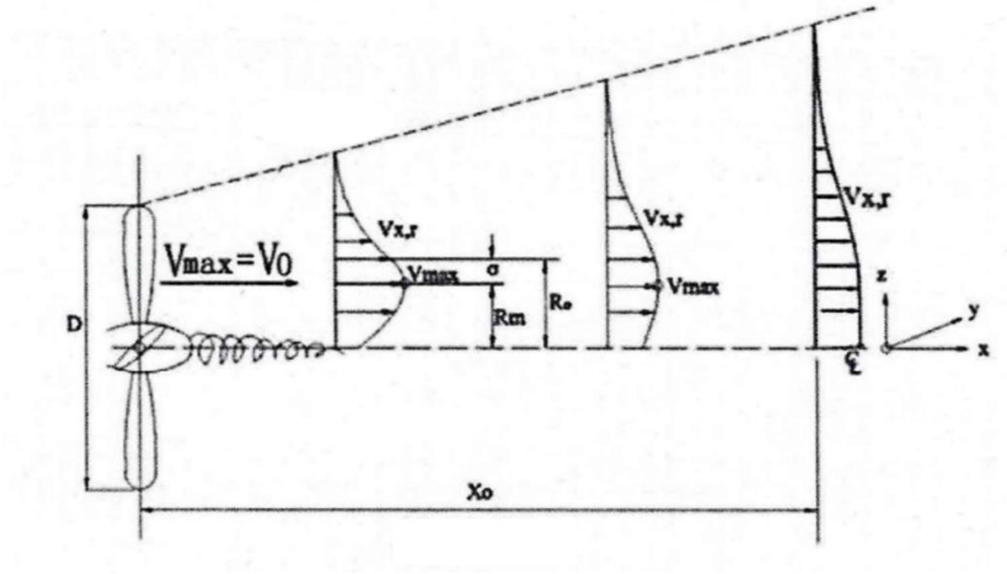

Figure 1 Axial velocity distribution

In 2012, Lam [9-10] systematically summarized the flow characteristics of the propeller jet without boundary effects by using physical experiments and numerical simulation methods, analyzed the three components of the jet velocity (axial, radial, and tangential) and discussed the attenuation and distribution of turbulence intensity in a propeller jet.

Although previous studies have studied the effect of the propeller jet shape and the bottom boundary on the initial flow velocity, the effect of the bottom boundary on the propeller jet shape has not been specifically studied. In present study, we used Star-ccm+ to study the CFD model of the propeller jet and simulated the change of the distance between the ship and the seabed in a still water field by changing the distance between the propeller and the bottom boundary. We observed the flow characteristics of the propeller jets at different distances from the boundary, including the axial, tangential and radial velocity distributions of the propeller jets.

1. Turbulence model

1.1 governing equations

For any complex turbulent motion, the N-S equation is applicable. The basic governing equation of an impressible viscous fluid is composed of a continuity equation and a RANS equation, and its tensor form is as followed:

$$\frac{\partial \rho}{\partial t}+\frac{\partial u_i}{\partial x_i}=0 \tag{1}$$

$$\frac{\partial}{\partial t}(\rho u_i)+\frac{\partial}{\partial x_j}(\rho u_i u_j)=-\frac{\partial P}{\partial x_i}+\frac{\partial}{\partial x_j}\left[u_0\left(\frac{\partial u_i}{\partial x_j}+\frac{\partial u_j}{\partial x_i}\right)-\frac{2}{3}\mu_0\frac{\partial u_k}{\partial x_k}\delta_{ij}\right]+\frac{\partial}{\partial x_j}\left(-\rho\overline{u_i' u_j'}\right)+\rho f_i \tag{2}$$

Where: ρ is the density of the fluid; p is the static pressure; f_i is the mass force per unit mass; u_i, u_j, u_k are velocity components; μ_0 is the molecular viscosity coefficient; $-\rho\overline{u_i' u_j'}$ is Turbulent Reynolds stress term due to time homogenization

1.2 Turbulence model

For numerical simulation of the unsteady hydrodynamic performance of propellers, researchers generally use the SST k-ω model [11]. The SST k-ω model combines the advantages of Standard k-ω and Standard k-ε turbulence models. Especially in star-ccm +, SST k-ω occupies a great advantage in the processing of boundary layers. The SST k-ω model uses turbulent kinetic energy k and dissipation rate ω as the solution variables. The transport equations for k and ω are as followed:

$$\frac{\partial}{\partial t}(\rho k)+\frac{\partial}{\partial x_i}(\rho k u_i)=\frac{\partial}{\partial x_j}\left(\Gamma_k\frac{\partial k}{\partial x_j}\right)+G_k-Y_k \tag{3}$$

$$\frac{\partial}{\partial t}(\rho\omega)+\frac{\partial}{\partial x_i}(\rho\omega u_i)=\frac{\partial}{\partial x_j}\left(\Gamma_\omega\frac{\partial \omega}{\partial x_j}\right)+G_\omega-Y_\omega+D_\omega \tag{4}$$

Where: k is the turbulent kinetic energy, ω is the dissipation rate; Γ_k and Γ_ω are the effective diffusion of k and ω, respectively; Y_k and Y_ω are the dissipation of k and ω, respectively; G_k and G_ω represent the generating terms of k and ω, D_ω Are cross-diffusion terms; S_k and S_ω are custom sources.

After enabling the SST k-ω model, the system will automatically enable the precise wall distnce and perform fully + processing on the wall.

2. Calculation model

2.1 Establishment of calculation model

Because the space shape of real ship propellers is very complex and what we studied in this paper was the flow field behind the propeller, the DTRC4119 propeller model was selected for analysis and calculation. The paddle dimensions are shown in Table 1.

Table 1 The paddle dimensions

Name	P4119
Diameter D_p （m）	0.305
Paddle number Z	3

Hub diameter ratio D_{hub}/D_p	0.2
Disk ratio A_E/A_o	0.60

The rectangular coordinate system O-xyz is used for modeling, the center of the propeller is the coordinate origin (0,0,0), the propeller rotation axis coincides with the X axis, and the positive direction of the X axis points downstream, which is the direction of water flow; The Z axis refers to the direction that from the center of the paddle surface to above the pool; the Y axis refers to the direction from the center of the paddle surface to the blade, obeying the right-hand spiral rule. The propeller model is shown in Figure 2.

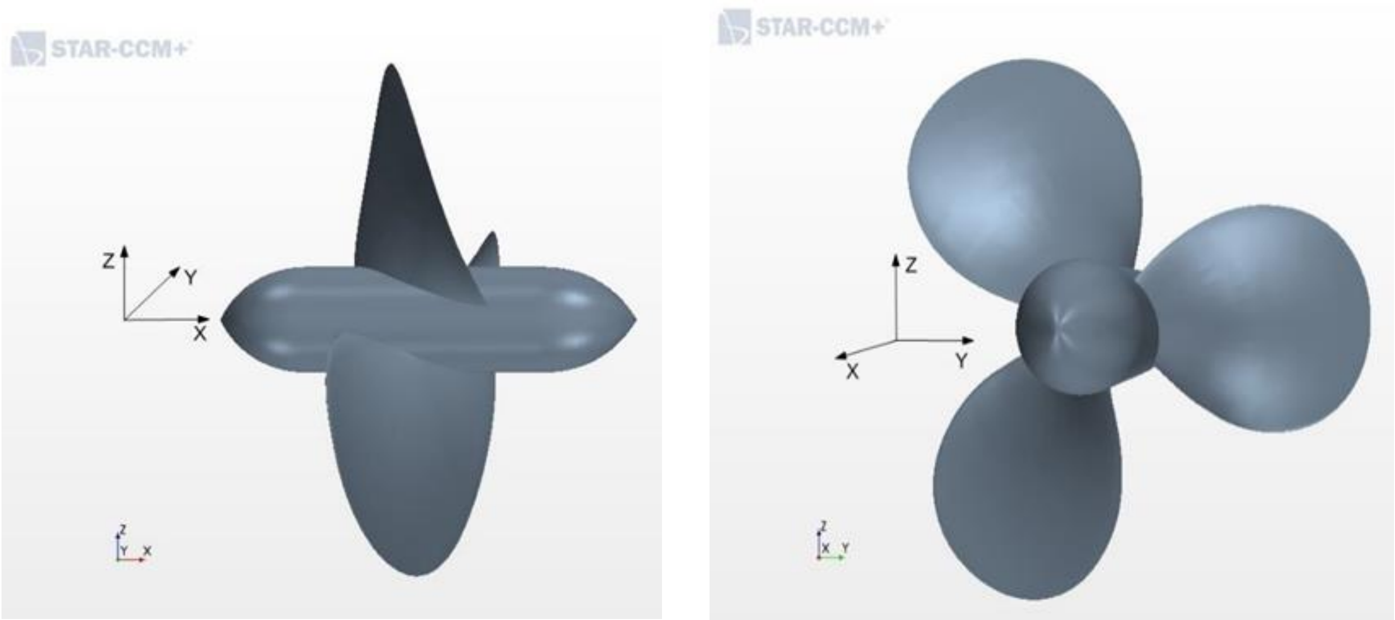

Figure 2 DTRC4119 propeller

The propeller rotation is modeled using a moving reference frame model, so the calculated flow field has two regions, one for the rotating propeller and the other for the static fluid domain. As shown in Figure 3, the cuboid was taken for the static area with 10Dp before the paddle, 1.5Dp after the paddle, 0.2Dp on the left and right, and 1.64Dp on the top and bottom. A cylinder is taken for the rotation area with the front and rear of the blade as 0.2Dp and the radius of 0.6Dp. The center axis of the cuboid and the cylinder coincides with the paddle axis, that is, coincides with the X axis.

Interface between the rotating area and the static area was established to transfer mass and energy during the calculation; the inlet boundary was set to the speed inlet, the outlet was set to the pressure outlet, and the hydro static pressure was set; the wall was set to sliding wall surface condition, and the displacement of the sliding wall surface relative to the fluid is zero, so there is no viscosity effect on the wall surface.

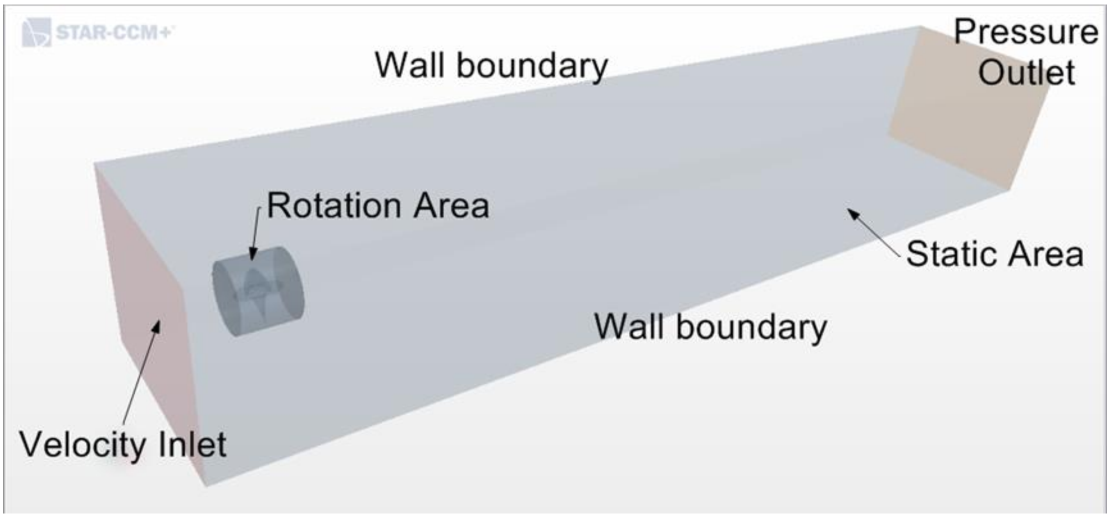

Figure 3 Computational domain

The cut volume grid was used to generate a mesh model for the computational domain. In consideration of computer performance and other issues, only the propeller and a certain area around it were encrypted. The static area used a relatively sparse grid size. Figure 4 is a cross-sectional view of XOZ, which can clearly see the partially encrypted part.

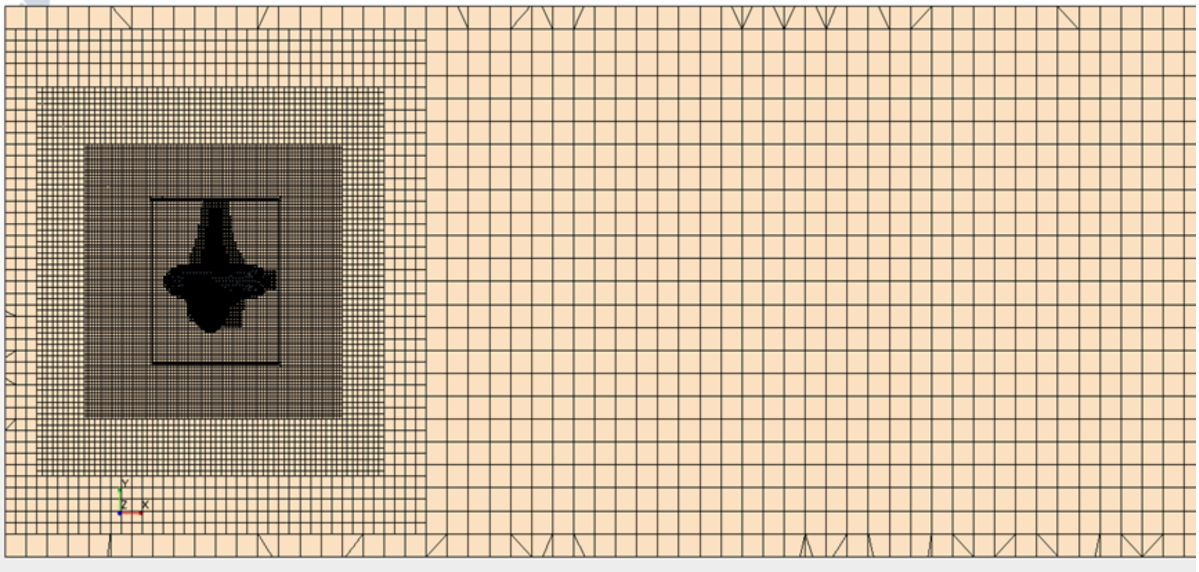

Figure 4 Grid cross section

2.2 Working condition setting

This article is to explore the flow characteristics of the propeller jet at different distances from the bottom boundary, so four different boundaries are set. The distance between the propeller shaft and the bottom boundary was denoted as z, which was set to 0.5, 0.4, 0.35, 0.3, respectively. The same speed, n = 900rpm, were set for 4 kinds of working conditions, taking the optimal value of the velocity coefficient J as 0.833, and the inlet velocity V0 = 3.81m / s. The Working condition setting table is shown in Table 2.

Table 2 Working condition setting table

Working condition	N	n	z	J	V_0
1	3	900	0.5	0.833	3.81
2	3	900	0.4	0.833	3.81
3	3	900	0.35	0.833	3.81
4	3	900	0.3	0.833	3.81

As shown in the figure 5, the propeller is placed at 0.5 m from the top surface, changing the distance between the propeller and the bottom boundary, z is 0.5, 0.4, 0.35, 0.35, 0.3.Z changes from 0.8 m to 1 m, x indicates the distance between the propeller and the disk along the axial direction of the propeller.

3. velocity field analysis

3.1 The efflux velocity

Figure 6 compares the axial velocity distribution on the initial plane at four different water depths. The maximum axial speeds at the four water depths are nearly equal, which means that in the initial plane (x/Dp=0), since the propeller speed is the same and the incoming flow speed is the same, the maximum axial speed is also the same. Water depth has no effect on it and axial velocity distribution peaks at z / Rp = ± 0.1

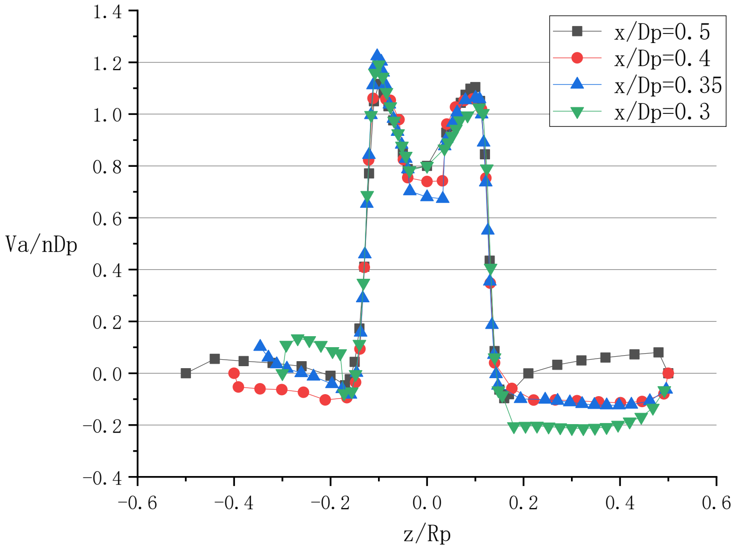

3.2 Axial speed on rotating shaft

In this paper, the axial velocities on the intersections of the y = 0 plane with the 6 sections (x / Dp = 0 / 0.05 / 0.13 / 0.27 / 0.46 / 0.78 / 1.42 / 2.13) are analyzed. Figure 7 compares the axial velocity at different boundary distances. Because the cross section at x / Dp = 0 or 0.05 passes through the hub, there is no speed at x / Dp = 0, the average of the two sides was taken for calculation. In the calculation domain of z = 0.5(Figure 7.a), the velocity generated by the propeller's rotation disturbing the water flow can be fully developed because it is not affected by the bottom boundary. Due to the high-speed rotation of the blade, the water flow velocity on both sides is increasing, so a double peak phenomenon occurs. The double-peak peak value has been decreasing since the x / Dp = 0 cross section, but the double-peak trend is obvious; at the x / Dp = 0.46 cross section, the double-peak trend is not obvious, and the velocity gradually shows a single-peak trend, but it is still asymmetrical, and the speed development zone changes to the speed completion zone; after that, it shows a single-peak trend with the maximum speed on the central axis until the speed is 0.

In the calculation domain of z = 0.4(Figure 7.b), from the initial plane to the cross section of x / Dp = 0.27, the peak value of the axial velocity, the double-peak trend, and the symmetrical shape are the same as those obtained in the calculation domain of z = 0.5. However, starting from the x / Dp = 0.27 cross section, the velocity on the central axis keeps increasing, making the double peaks become single peaks, and the peak of the water velocity near the bottom boundary below the central axis is slightly higher than the central axis. At the x / Dp = 0.78 cross section, when z / Rp = 0.059, the speed reaches the peak Va / nDp = 0.575, but on the other side, when z / Rp = 0.059, the speed reaches the peak Va / nDp = 0.738, and the peak speed of the lower side was 28.3% higher than the upper side.

As the distance from the bottom boundary decreases, the phenomenon mentioned above becomes more obvious. In the calculation domain of z = 0.35(Figure 7.c), at the x / Dp = 0.39 cross section, when z / Rp = 0, the velocity reaches the peak Va / n Dp = 0.78, but on the other side, when z / Rp = -0.061, the velocity reaches the peak Va / n Dp = 0.94, and the peak speed of the lower side was 20.5% higher than the upper side; at the x / Dp = 0.78 cross section, when z / Rp = 0.0325, the speed reaches the peak Va / n Dp = 0.7, but on the other side, when z / Rp = -0.014, the speed reaches the peak Va / n Dp = 0.81, and the peak speed of the lower side is 28.3% higher than the upper side, and the peak speed of the lower side was 15.7% higher than the upper side.

In the calculation domain of z = 0.3(Figure 7.d), at the x / Dp = 0.39 cross section, when z / Rp = 0.012, the velocity reaches the peak Va / n Dp = 0.78, but on the other side, when z / Rp = -0.076, the velocity reaches the peak Va / n Dp =1.05, and the peak speed of the lower side was 34.6% higher than the upper side. What's more, in the calculation domain of z = 0.3, starting from the cross section of x / Dp = 0.39, a single peak appears in the velocity, and the peak is at the position z / Rp = -0.076 below the center axis.

When the distance from the bottom boundary is reduced, the water flow is restricted by the bottom boundary and cannot be fully developed, and the axial velocity of the water flow is greatly affected. The closer the propeller is to the bottom boundary, the more unstable the symmetric shape of the axial velocity is, the more the peak value of the single peak velocity is biased toward the bottom boundary, and the greater the speed near the wall is.

(a) z=0.5

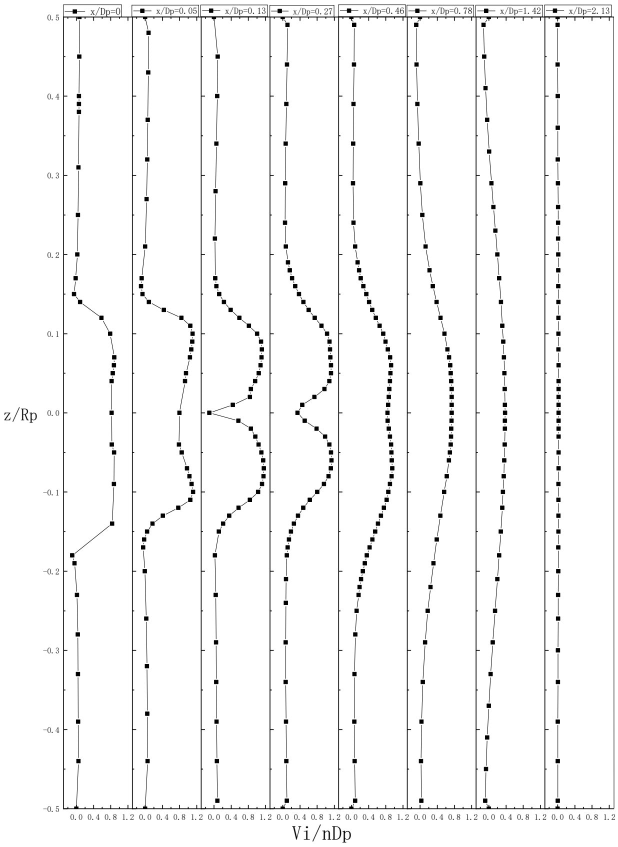
x/Dp=0
x/Dp=0.05
x/Dp=0.13
x/Dp=0.27
x/Dp=0.46
x/Dp=0.78
x/Dp=1.42
x/Dp=2.13
z/Rp
0.5
0.4
0.3
0.2
0.1
0.0
-0.1
-0.2
-0.3
-0.4
-0.5
0.0 0.4 0.8 1.2
Vi/nDp

(b) z=0.4

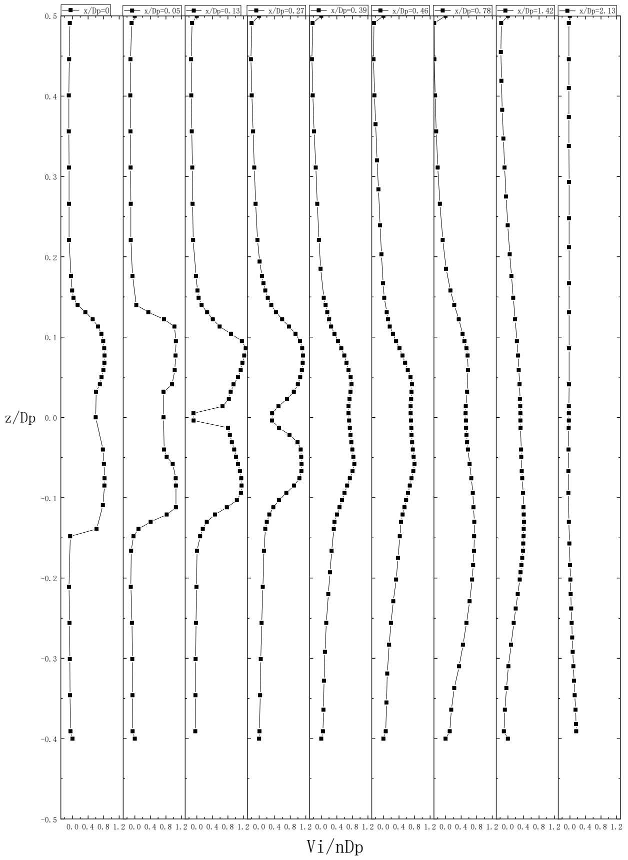
x/Dp=0
x/Dp=0.05
x/Dp=0.13
x/Dp=0.27
x/Dp=0.39
x/Dp=0.46
x/Dp=0.78
x/Dp=1.42
x/Dp=2.13
z/Dp
0.5
0.4
0.3
0.2
0.1
0.0
-0.1
-0.2
-0.3
-0.4
-0.5
0.0 0.4 0.8 1.2
Vi/nDp

(c) z=0.35

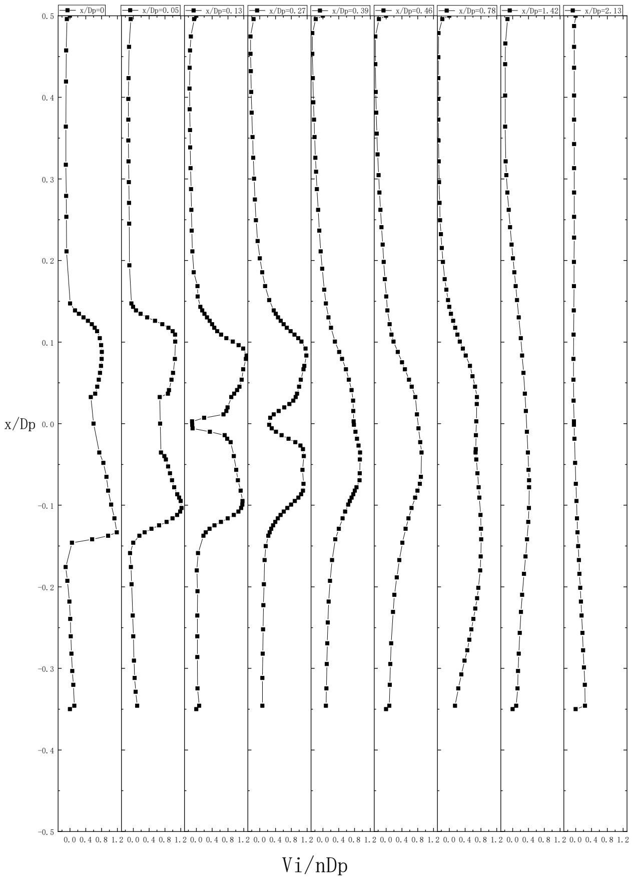
x/Dp=0
x/Dp=0.05
x/Dp=0.13
x/Dp=0.27
x/Dp=0.39
x/Dp=0.46
x/Dp=0.78
x/Dp=1.42
x/Dp=2.13
0.5
0.4
0.3
0.2
0.1
0.0
-0.1
-0.2
-0.3
-0.4
-0.5
x/Dp
0.0 0.4 0.8 1.2
Vi/nDp

(d) z=0.3

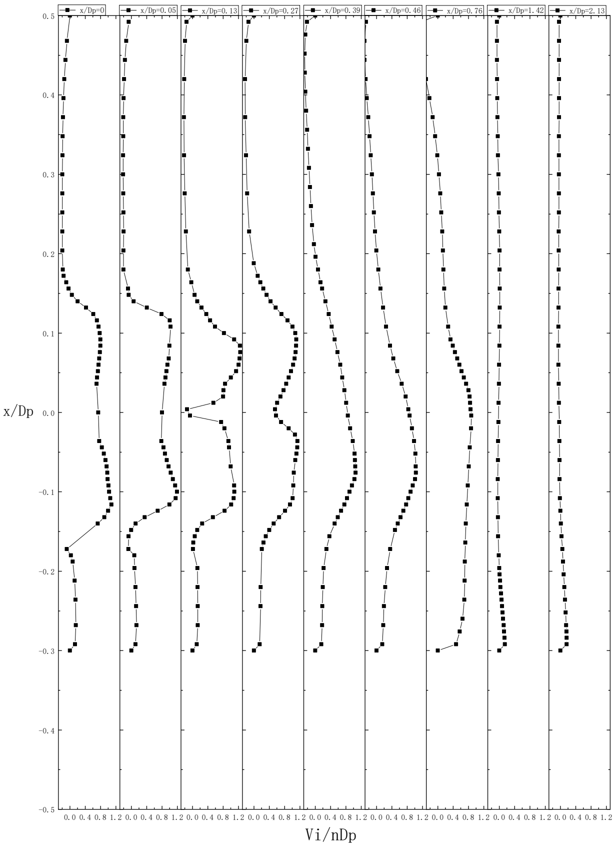
x/Dp=0
x/Dp=0.05
x/Dp=0.13
x/Dp=0.27
x/Dp=0.39
x/Dp=0.46
x/Dp=0.76
x/Dp=1.42
x/Dp=2.13
0.5
0.4
0.3
0.2
0.1
0.0
-0.1
-0.2
-0.3
-0.4
-0.5
x/Dp
0.0 0.4 0.8 1.2
Vi/nDp

Figure 7 Comparison of axial velocities at different boundary distances: (a) z =0.5; (b) z =0.4; (c) z =0.35; (d) z =0.3

3.3 Tangential velocity

The rotating propeller has a disturbing action on the stationary fluid, causing the fluid to perform a rotational movement following the rotation of the propeller, resulting in a tangential velocity. Because the simulation experiment is in a static flow field, the tangential component of the velocity in the water flow is only generated by the rotation of the propeller.

Figure 8.a is the tangential velocity distribution on different cross sections in the calculation domain of z = 0.5. Currently, the bottom boundary has no effect on the development of tangential velocity. At the x / Dp = 0.13 cross section, the tangential velocity reaches its peak. The disturbance of the hub has a great influence on the flow field, and there are peaks in both positive and negative directions around Z / RP = 0. At the same time, the rotation of the flow field near the leaf tip is also obvious, and there are also peaks in both positive and negative directions around z / Rp = 1. In the calculation domain of z = 0.5, the tangential component of the velocity of the water flow field is symmetrical about the center of the rotation axis, and the tangential velocity decreases rapidly along the center axis. At the x / Dp = 1.42 cross section, the tangential velocity is already close to 0.

Contrast the tangential velocity components in the four calculation domains of z = 0.5, z = 0.4, z = 0.35, and z = 0.3, show as Figure 8, under the influence of the bottom boundary, the closer it is to the bottom boundary, the greater the influence of the wave on the tangential velocity is. At the x / Dp=0.39 cross section, the absolute value of the velocity peak near one side of the bottom boundary is not as large as at the other side; at the x / Dp = 0.78 cross section, the velocity profile about the center symmetry can no longer be maintained, and the tangential velocity changes into a unimodal curve. But at the x / Dp = 1.42 cross section, the phenomenon that the tangential velocity is close to 0 remains unchanged.

(a) z =0.5

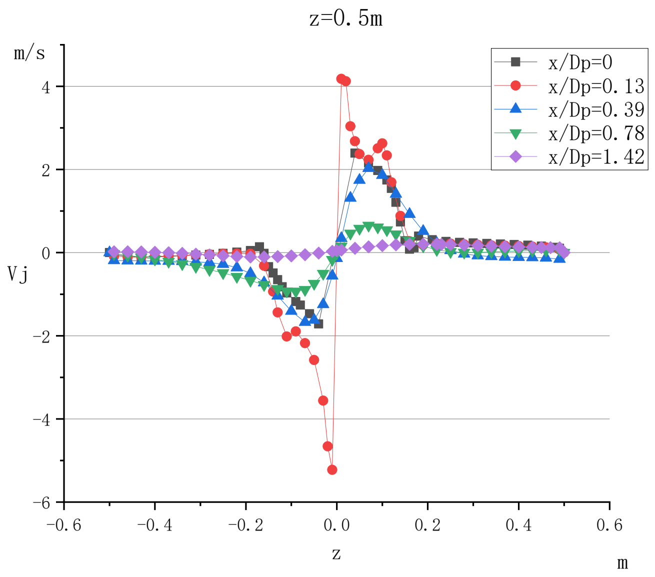

(b) z =0.4

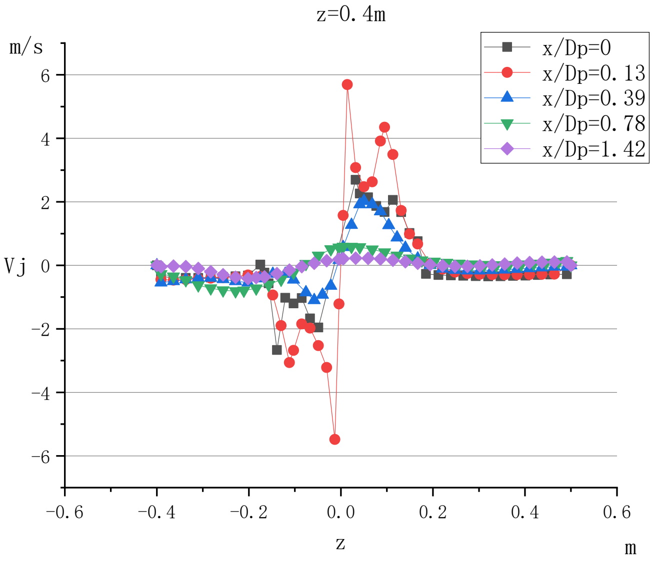
z=0.4m
m/s
Vj
z
m
x/Dp=0
x/Dp=0.13
x/Dp=0.39
x/Dp=0.78
x/Dp=1.42
6
4
2
0
-2
-4
-6
-0.6
-0.4
-0.2
0.0
0.2
0.4
0.6

(c) z =0.35

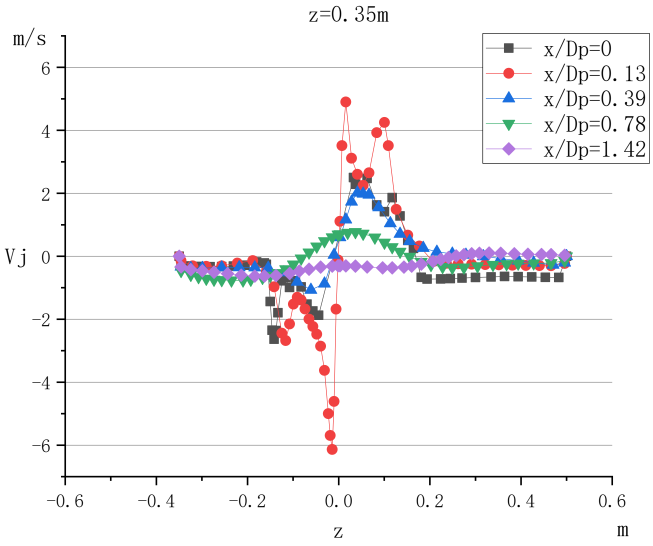
z=0.35m
m/s
Vj
z
m
x/Dp=0
x/Dp=0.13
x/Dp=0.39
x/Dp=0.78
x/Dp=1.42
6
4
2
0
-2
-4
-6
-0.6
-0.4
-0.2
0.0
0.2
0.4
0.6

(d) z =0.3

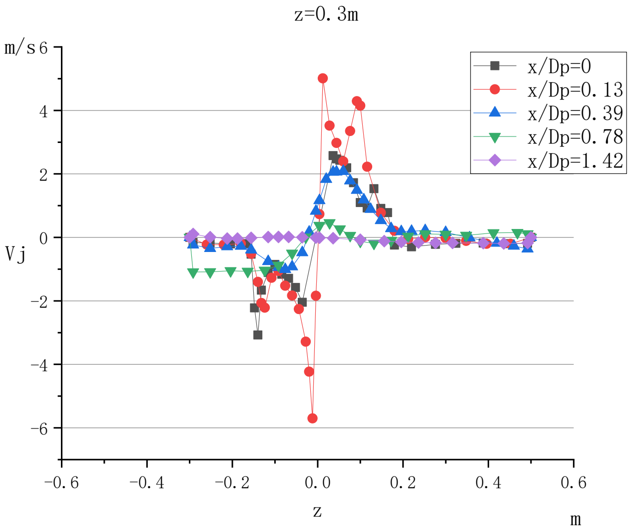
z=0.3m
m/s
Vj
z
m
x/Dp=0
x/Dp=0.13
x/Dp=0.39
x/Dp=0.78
x/Dp=1.42
6
4
2
0
-2
-4
-6
-0.6
-0.4
-0.2
0.0
0.2
0.4
0.6

Figure 8 Comparison of tangential velocities at different boundary distances: (a) z =0.5; (b) z =0.4; (c) z =0.35; (d) z =0.3

3.4 Radial velocity

In our study, the simulated radial velocity of the initial plane (Figure 9) also has a peak, but it is to the left of the paddle axis and rapidly decreases to the blade tip. Comparing the radial velocity components in the four calculation domains of z = 0.5, z = 0.4, z = 0.35, and z = 0.3, it can be seen that the hub and blade tip have a great influence on the radial component of the jet at the initial plane. In the four calculation domains, the radial velocity reaches the maximum value in the initial plane, but it decreases rapidly due to the influence of the hub rotation. The influence of the bottom boundary on the radial velocity is that the closer the propeller is to the bottom boundary, the larger the radial velocity fluctuation will be. However, after the x / Dp = 0.13 cross section, the radial velocity itself is very small and its contribution to the velocity is small, so it can be ignored.

(a) z =0.5

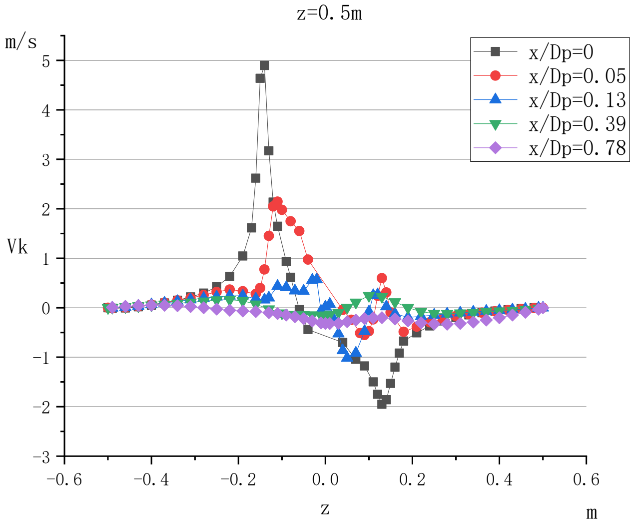

(b) z =0.4

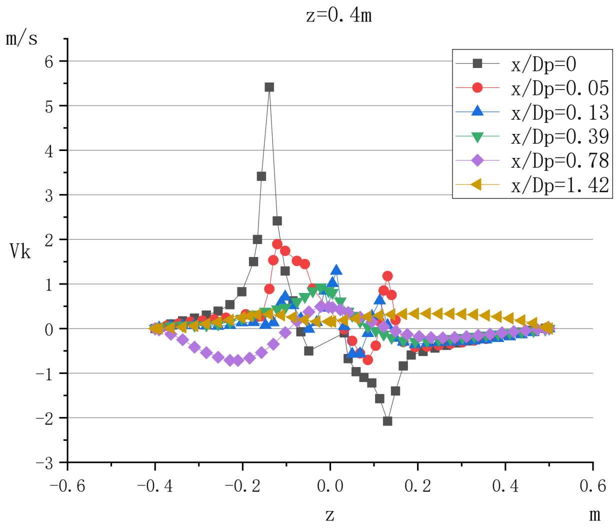

(c) z =0.35

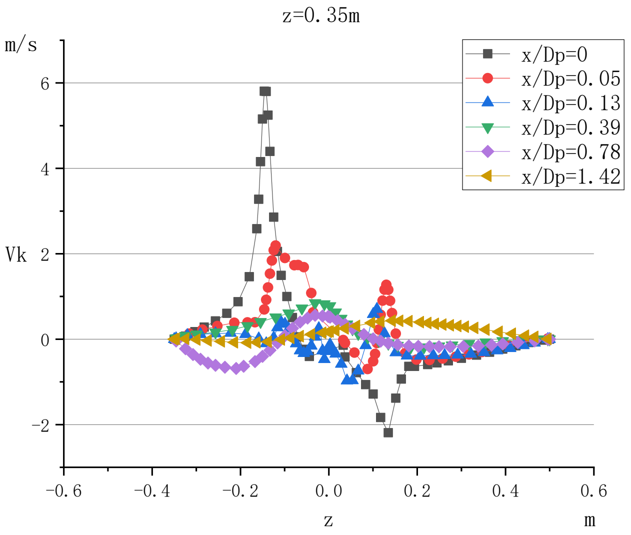

(d) z =0.3

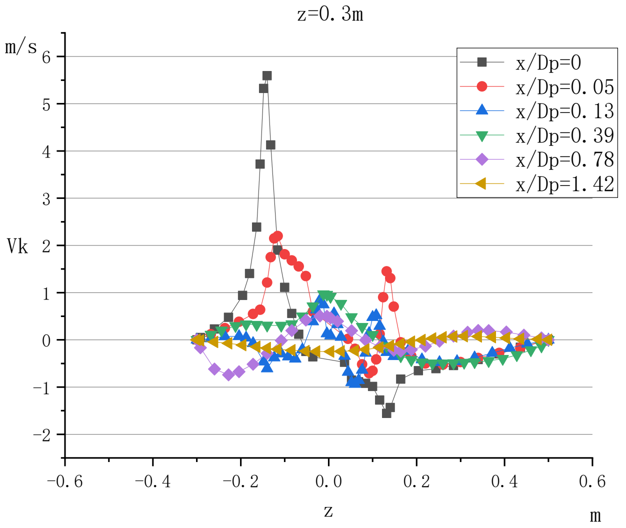

Figure 9 Comparison of radial velocities at different boundary distances: (a) z =0.5; (b) z =0.4; (c) z =0.35; (d) z =0.3

Conclusion

In our study, we used the CFD simulation software Star-ccm + to verify the propeller jet velocity. Comparing the results of this simulation with those of previous studies, we found that Star-ccm + can be applied to the numerical simulation of propeller jets. In addition, We studied the velocity of the propeller jet in a flow field at different distances from the bottom boundary, and reached the following conclusions:

1. The simulation results show that the distance from the bottom boundary on the initial plane cannot affect the size and position of the initial velocity;

2. Through the comparison of 4 different flow fields, in the development zone, the closer to the bottom boundary, the smaller the range of the development zone, the more the single-peak velocity peak on the development completed area is biased towards the bottom boundary,

and the near wall velocity is greater.

3. For the tangential component of the jet velocity, in the jet development zone, the closer to the bottom boundary, the smaller the peak value on the side near the bottom boundary, and in the development completion zone, the closer it is to the bottom boundary, the earlier it changes from a central symmetrical velocity pattern to a single peak velocity pattern. For the radial component of the jet velocity, after the initial plane, the closer to the bottom boundary, the greater the fluctuation in radial velocity. However, because the radial velocity is small, the effect on the velocity of the flow field can be ignored.

References

1. Zheng Tian-li. Harm and engineering measures of marine propellers and boosters on port hydraulic structures [J]. Water Transport Engineering, 2001 (7): 29-32.
2. ALBERTSON M L , DAI Y B , JENSEN R A , et al . Diffusion of submerged jets[J]. J Transcript of the ASCE, 1993, 115(1):639-664.
3. Whitehouse R. scour at marine structures: a manual for practical applications. Thomas Tedford publisher, 1998.
4. Sumer B M , Freese J . The Mechanics of Scour in the Marine Environment[J]. 2002.
5. Stewart, James D P . Characteristics of a ship's screw wash and the influence of quay wall proximity.[J]. Queens University of Belfast, 1992.
6. Hamill G A , Johnston H T . The decay of maximum velocity within the initial stages of a propeller wash[J]. Journal of Hydraulic Research, 1993, 31(5):605-613.
7. HASHMI H N . Erosion of a granular bed at a quay wall by a ship' s screw wash[D] Northern Ireland: Queen' s University of Belfast ,1993.
8. Lam W , Hamill G A , Song Y C , et al. A review of the equations used to predict the velocity distribution within a ship’s propeller jet[J]. Ocean Engineering, 2011, 38(1):1-10.
9. Lam W H , Hamill G , Robinson D , et al. Analysis of the 3D zone of flow establishment from a ship’s propeller[J]. Ksce Journal of Civil Engineering, 2012, 16(4):465-477.
10. Lam W H , Robinson D J , Hamill G A , et al. An effective method for comparing the turbulence intensity from LDA measurements and CFD predictions within a ship propeller jet[J]. Ocean Engineering, 2012, 52(none).
11. Kong Jinping, Wu Bo-tao, Kong Ling-zhi. Analysis of hydrodynamic performance of ship's twin propellers based on CFD [J]. Ship Science and Technology, 2019 (5).